The Local Structure of Atmospheric Turbulence and Its Effect on the Smagorinsky Model for Large Eddy Simulation

MARCELO CHAMECKI

Department of Geography and Environmental Engineering, and Center for Environmental and Applied Fluid Mechanics, The Johns Hopkins University, Baltimore, Maryland

CHARLES MENEVEAU

Department of Mechanical Engineering, and Center for Environmental and Applied Fluid Mechanics, The Johns Hopkins University, Baltimore, Maryland

MARC B. PARLANGE

School of Architecture, Civil, and Environmental Engineering, Ecole Polytechnique Fédérale de Lausanne, Lausanne, Switzerland

(Manuscript received 25 May 2006, in final form 11 September 2006)

ABSTRACT

Phenomena such as large-scale shear, buoyancy, and the proximity to the ground surface significantly affect interactions among scales in atmospheric boundary layer turbulent flows. Hence, these phenomena impact parameters that enter subgrid-scale (SGS) parameterizations used in large eddy simulations (LES) of the atmospheric boundary layer. The effects of these phenomena upon SGS parameters have, to date, been studied mostly as functions of the global state of the flow. For instance, the Smagorinsky coefficient has been measured as a function of the mean shear and stability condition of the atmosphere as determined from the average surface heat and momentum fluxes. However, in LES the global average field values are often difficult to determine a priori and the SGS parameters ideally must be expressed as a function of local flow variables that characterize the instantaneous flow phenomena. With the goal of improving the Smagorinsky closure, in this study several dimensionless parameters characterizing the local structure and important dynamical characteristics of the flow are defined. These local parameters include enstrophy, vortex stretching, self-amplification of strain rate, and normalized temperature gradient and all are defined in such a way that they remain bounded under all circumstances. The dependence of the Smagorinsky coefficient on these local parameters is studied a priori from field data measured in the atmospheric surface layer and, as a reference point, from direct numerical simulation of neutrally buoyant, isotropic turbulence. To capture the local effects in a statistically meaningful fashion, conditional averaging is used. Results show various important and interrelated trends, such as significant increases of the coefficient in regions of large strain-rate self-amplification and vortex stretching. Results also show that the joint dependence on the parameters is rather complicated and cannot be described by products of functions that depend on single parameters. Dependence on locally defined parameters is expected to improve the SGS model by sensitizing it to local flow conditions and by enabling possible generalizations of the dynamic model based on conditional averaging.

1. Introduction

Large eddy simulation (LES) has evolved into a powerful tool to perform the numerical simulation of high Reynolds number turbulent flows. The LES technique originated from meteorological applications with the works of Smagorinsky (1963) and Lilly (1967). Simulations of the atmospheric boundary layer (ABL) were first performed by Deardorff (1972, 1974) and Moeng (1984) and are currently of crucial importance to improve our understanding of turbulent transport in the ABL.

In LES, the larger scales are explicitly resolved while

Corresponding author address: Charles Meneveau, Department of Mechanical Engineering, The Johns Hopkins University, Baltimore, MD 21218.
E-mail: meneveau@jhu.edu

DOI: 10.1175/JAS3930.1

the effect of the smaller ones is represented through the subgrid-scale (SGS) stress tensor, which involves unknown quantities and has to be parameterized. One of the simplest approaches is based on the concept of turbulent viscosity, introduced by Boussinesq (1877) and first applied to LES by Smagorinsky (1963). By analogy with the molecular viscosity, the SGS stress tensor is assumed to be proportional to the resolved strain-rate tensor. The proportionality is given through a turbulent (or eddy) viscosity ν_T, which is then modeled using a mixing length approach

$$\nu_T = l^2|\tilde{\mathbf{S}}| = (c_s\Delta)^2|\tilde{\mathbf{S}}|. \quad (1)$$

Here $l = c_s\Delta$ is the mixing length, Δ is the filter width, $(\sim)$ represents the filtering operation, c_s is the Smagorinsky coefficient, and $|\tilde{\mathbf{S}}| = (2\tilde{S}_{ij}\tilde{S}_{ij})^{1/2}$ is the magnitude of the resolved strain-rate tensor defined as $\tilde{S}_{ij} = 1/2(\partial_j\tilde{u}_i + \partial_i\tilde{u}_j)$. By assuming that the filter is within the inertial subrange (where Kolmogorov scaling is valid) and that the average SGS dissipation has to match the viscous dissipation, Lilly (1967) determined the value of the coefficient to be $c_s \approx 0.17$.

Despite extensive work documenting shortcomings of the Smagorinsky model in representing the SGS stress tensor (see Clark et al. 1979; Bardina et al. 1980; Mason 1994; Meneveau and Katz 2000; Tao et al. 2002), it is still widely used in LES because of its simplicity and attractive numerical properties. However, for the Smagorinsky–Lilly model to yield good results in simulations of the ABL, three main (and maybe related) issues have to be considered. The first one is related to the occurrence of strong mean velocity gradients (usually close to the ground). The basic idea behind the model (1) is that the turbulent eddy viscosity is proportional to the resolved turbulent velocity gradients (Mason 1994). In regions where the mean velocity gradients are comparable to the turbulent ones, the viscosity obtained from the model is too high. An alternative implementation where the model is based only on the turbulent component of $\tilde{\mathbf{S}}$ was proposed by Schumann (1975) and a modified version specific for the ABL is the model proposed by Sullivan et al. (1994). Both models require evaluation of the mean velocity gradients.

Another challenge is that, close to the ground, the turbulence integral scale decreases and becomes comparable to the filter scale (see Mason 1994). In this region Lilly's hypotheses are no longer valid, the filter width is no longer a good estimate for the mixing length, and not even the mechanisms of production of turbulent kinetic energy are well resolved (Kosovic 1997). Once again the Smagorinsky model overestimates the eddy viscosity. Mason (1994) proposed a modified mixing length that matches the Smagorinsky one far from the ground and the rough-surface expression for eddy viscosity near the ground.

The last issue is related to the effects of buoyancy on the eddy viscosity. Although such effects can be neglected when the filter is within the inertial range (Mason 1994), this is not the case close to the ground. Mason suggests a modified eddy viscosity that accounts for the effects of (mean) buoyancy on the integral scale and on the energy balance. Canuto and Cheng (1997) derive a mixing length expression that accounts for both mean buoyancy and mean shear effects. A convenient approach to account for the changes in the eddy viscosity due to these three factors consists of keeping the functional form (1) unchanged and adjusting the Smagorinsky coefficient. Experimental analysis of atmospheric data by Kleissl et al. (2003) and Sullivan et al. (2003) shows that the coefficient has to be greatly reduced when the atmosphere has a stable structure (i.e., when buoyancy acts to suppress turbulence). Kleissl et al. (2003) presented an empirical function to describe the global effects of buoyancy and distance from the ground on the coefficient. This function [Eq. (14) in Kleissl et al. (2003)] is written as the product of two functions each separately describing dependence on stability and distance from the ground.

Most of the approaches described so far attempt to determine a functional dependence between the eddy viscosity parameter and parameters characterizing mean shear, mean buoyancy, distance from the ground, etc. However, mean quantities are not known a priori during a simulation. For nonhomogeneous flow geometries, accumulating such averages during LES is a challenge. A more general approach to deal with nonhomogeneous complex-physics flows is the dynamic model proposed by Germano et al. (1991). In principle, this model allows for the temporal and spatial variability of the coefficient and can reproduce nontrivial dependence on the flow conditions. In the dynamic model the coefficient is determined during the simulation based on the smallest resolved scales (adopting a scale-similarity hypothesis). For ABL applications, scale similarity does not hold close to the surface and Porté-Agel et al. (2000) developed a scale-dependent dynamic model, which yields good results at the cost of an additional filtering operation. Kleissl et al. (2004) used a priori tests with data measured in the atmospheric surface layer to show that a scale-dependent dynamic model is also capable of reproducing many of the effects of atmospheric stability as characterized using global average heat and momentum fluxes. This has been confirmed in a posteriori tests performed by

Kleissl et al. (2006) and Kumar et al. (2006), who used the scale-dependent Lagrangian dynamic model (Bou-Zeid et al. 2005).

Another important consideration is the influence of coherent structures on the optimal value for the Smagorinsky coefficient. Recent work by Kang and Meneveau (2005) documented the effects of coherent structures (periodic vortices) in a cylinder wake upon the SGS stress tensor. Their results suggest that the Smagorinsky model should perform better in the high-strain regions between coherent vortices than within the vortices themselves. However, it is not known whether this conclusion is valid in the context of ABL flows. Also there are no "periodic" von Kármán vortices in the ABL, where the identification of vortical structures is therefore more problematic. Lin (1999), Porté-Agel et al. (2001a,b), and Carper and Porté-Agel (2004) studied the effect of sweeps and ejections on the SGS energy fluxes in the atmospheric surface layer. Kobayashi (2005) proposed a modified Smagorinsky model that is sensitive to the effect of coherent structures. In his model, the Smagorinsky coefficient has a functional dependence on a local parameter that identifies the coherent structures. As is apparent from this discussion, other than these few earlier studies, there is little direct empirical evidence documenting the dependence of the Smagorinsky coefficient on local parameters characterizing ABL flow.

The main objective of the present study is to quantify the dependence of the Smagorinsky coefficient upon *local* parameters of the *resolved* scales. It is important to note that such parameters are typically available during the simulations and can be directly incorporated in the SGS model. Specifically, one would like to write

$$c_s^2 = f(\Pi_1, \Pi_2, \ldots), \tag{2}$$

where the Πs are physically relevant parameters. Two basic issues are raised by this objective. The first is to identify a set of physically meaningful local flow parameters, Π_k. For dimensional consistency they must be dimensionless. The parameters thus typically involve ratios of two locally determined flow variables. Hence, particular attention must be devoted to formulations that avoid divisions by zero. This can be satisfied if the dimensionless parameters are formally bounded by construction. The second issue relates to how to characterize the dependence of the Smagorinsky coefficient upon local flow parameters in a statistically meaningful fashion (i.e., without having trends hidden by the natural high variability that occurs inherently in turbulence data). The tool to be used will be conditional averaging, that is, the coefficient will be sought for specified value ranges of the set of dimensionless flow parameters. These two issues are addressed in section 2, where the parameters to be studied are defined and where the conditional averaging to be used to analyze data is explained. In section 3 the dataset as well as the general data analysis procedures are described. Results are presented in section 4 and further discussed in section 5.

2. Flow parameters and averaging

a. Local flow parameters

The first parameters to be considered describe effects of atmospheric stability and distance from the ground. These effects on the eddy viscosity and Smagorinsky coefficient have been extensively studied (e.g., Mason 1994; Canuto and Cheng 1997) and experimentally documented (Kleissl et al. 2003; Sullivan et al. 2003). Kleissl et al. used Δ/z (z is the distance from the surface) and Δ/L (L is the Obukhov length obtained through time averaging) to characterize distance from the ground and buoyancy, respectively. Sullivan et al. used only one parameter Λ_w/Δ (Λ_w being the wavelength of the peak in the vertical velocity spectrum) to describe both effects. Both studies led to the same conclusion—that the coefficient must be strongly reduced as the atmosphere changes from unstable to stable mean stratification.

Although both descriptions are capable of capturing stability effects, the parameters used are not locally defined and require averaging to determine L, Λ_w, etc. A possible alternative is to use the gradient Richardson number involving gradients. The traditional gradient Richardson number can be written in terms of local gradients of the filtered fields, according to

$$\mathrm{Ri}_g = \frac{(g/\tilde{T})(\partial\tilde{T}/\partial z)}{(\partial\tilde{u}/\partial z)^2 + (\partial\tilde{v}/\partial z)^2}, \tag{3}$$

where $\tilde{T}$ is resolved temperature, g is gravitational acceleration, and $\tilde{u}$, $\tilde{v}$ are the resolved horizontal velocities while z is, as usual, the vertical coordinate. Written in this local fashion, the Richardson number is more problematic than when it is written in a global sense. It is not a Galilean invariant expression. Locally, all the components of the velocity gradient tensor may have similar magnitudes and the tensor cannot be characterized by only two single components. Instead, it is preferable to define the Richardson number in the more general way suggested by Majda and Shefter (1998). Here their definition is used with temperature replacing density (invoking Boussinesq approximation) and multiplying the final result by a factor of 2 in order to match the critical stability value of ¼ for the usual definition (3):

$$\mathrm{Ri} = \frac{-2\mathbf{g}\cdot\boldsymbol{\nabla}\tilde{T}}{\tilde{T}(|\tilde{\mathbf{S}}|^2 + |\tilde{\boldsymbol{\omega}}|^2)}. \tag{4}$$

In Eq. (4), $|\tilde{\boldsymbol{\omega}}|^2$ is the magnitude of vorticity ($\tilde{\boldsymbol{\omega}} = \boldsymbol{\nabla}\times\tilde{\mathbf{u}}$). Note that this definition is invariant under Galilean transformations of the frame of reference.

Next, it is useful to follow Kleissl et al. (2003) and also use Δ/z to characterize the distance from the surface. The parameter Δ/z should be formally written as Δ/d_s, where d_s is the smallest distance between the point where the SGS stress is being modeled and the surface. In this way, the formulation fits complex geometries and the parameter is also independent of the frame of reference adopted. In this work both definitions are equivalent and Δ/z will be used for simplicity.

To further characterize the local structure of the resolved turbulent flow field, additional parameters based on the invariants of the local velocity gradient tensor are considered. There is ample evidence that these invariants are intrinsically related to the dynamics of turbulence (Chong et al. 1990; Martín et al. 1998). The five independent invariants of the velocity gradient tensor are given by (Pope 1975; Martín et al. 1998):

$$\begin{aligned}
I_1 &= |\tilde{\mathbf{S}}|^2 = 2\tilde{S}_{ij}\tilde{S}_{ji}\\
I_2 &= \mathrm{Det}(\tilde{\mathbf{S}}) = 3\tilde{S}_{ij}\tilde{S}_{jk}\tilde{S}_{ki}\\
I_3 &= |\tilde{\boldsymbol{\omega}}|^2 = \tilde{\omega}_i\tilde{\omega}_i\\
I_4 &= |\tilde{\mathbf{S}}\cdot\tilde{\boldsymbol{\omega}}|^2 = \tilde{\omega}_i\tilde{S}_{ij}\tilde{\omega}_k\tilde{S}_{kj}\\
I_5 &= \tilde{\boldsymbol{\omega}}\cdot(\tilde{\mathbf{S}}\cdot\tilde{\boldsymbol{\omega}}) = \tilde{\omega}_i\tilde{S}_{ij}\tilde{\omega}_j.
\end{aligned} \tag{5}$$

Note that all these invariants are related to important characteristics and processes of the resolved flow field: I_1 is the strain-rate magnitude, I_2 is related to self-amplification of strain rate, I_3 is the magnitude of vorticity (enstrophy), I_4 is the magnitude of the vortex stretching vector, and I_5 is the vortex stretching.

Borue and Orszag (1998) found that for isotropic turbulence the SGS dissipation predicted by the tensor eddy viscosity model is highly correlated to the measured SGS dissipation. They noted that the dissipation of the model is a linear combination of the second and fifth invariants (I_2 and I_5) and concluded that the SGS dissipation is strongly affected by these invariants. The SGS dissipation produced by the Smagorinsky model contains only information on the first invariant. Moreover, the dependence of the Smagorinsky coefficient upon the invariants (5) is theoretically justified in the more general nonlinear relation between stress and velocity gradients proposed by Pope (1975). Lund and Novikov (1992, 29–43) used a priori analysis to study the dependences of the expansion coefficients on the invariants in the context of LES defining four dimensionless parameters based on the invariants. They concluded that the dependences were too weak to explain the scatter and the low correlation observed in the a priori tests. In the present work, as explained in the next subsection, the effect of the parameters will be diagnosed using conditional averages rather than correlations and scatterplots as used in Lund and Novikov (1992, 29–43).

Since the Smagorinsky coefficient is dimensionless, it should depend only on dimensionless parameters, so the next challenge is to render the five invariants I_k dimensionless. Since only time scales are involved, the five invariants can be reduced to four dimensionless ones using one or several of them appropriately in denominators. As a criterion, we require that resulting parameters be bounded between -1 and 1, or between 0 and 1. Combining these requirements with the dynamical interpretations of the invariants described above, the following arrangement is proposed:

$$\begin{aligned}
S^* &= \frac{-12\sqrt{3}\mathrm{Det}(\tilde{\mathbf{S}})}{|\tilde{\mathbf{S}}|^3} \qquad Q^* = \frac{|\tilde{\boldsymbol{\omega}}|^2 - |\tilde{\mathbf{S}}|^2}{|\tilde{\boldsymbol{\omega}}|^2 + |\tilde{\mathbf{S}}|^2}\\
V^* &= \frac{3|\tilde{\mathbf{S}}\cdot\tilde{\boldsymbol{\omega}}|^2}{|\tilde{\boldsymbol{\omega}}|^2|\tilde{\mathbf{S}}|^2} \qquad W^* = \frac{\tilde{\boldsymbol{\omega}}\cdot(\tilde{\mathbf{S}}\cdot\tilde{\boldsymbol{\omega}})}{|\tilde{\boldsymbol{\omega}}||\tilde{\mathbf{S}}\cdot\tilde{\boldsymbol{\omega}}|}.
\end{aligned} \tag{6}$$

The first parameter (S^*) was introduced by Lund and Rogers (1994) to classify the local strain state of the flow field and has been frequently used in studies of LES (Tao et al. 2002; Higgins et al. 2003; Kang and Meneveau 2005; Chumakov 2006). The parameter S^* is bounded between -1 and 1 and indicates the type of deformation of the flow (e.g., -1 corresponds to axisymmetric contraction, 0 to plane shear, and 1 to axisymmetric extension).

The parameter Q^* is a measure of the relative magnitudes of strain and vorticity and is the base of the SGS model proposed by Kobayashi (2005). It is a dimensionless form of the second invariant of the full velocity gradient tensor (Q), frequently used to characterize flow topology (Chong et al. 1990; Martín et al. 1998). It is also known as the Q-criterion, proposed by Hunt et al. (1988) to identify vortical structures in turbulent flows. The Q^* is bounded between -1 and 1 and is positive in vorticity-dominated regions and negative in strain-dominated regions.

The third parameter, V^*, is a measure of the magnitude of the vortex stretching vector that plays a fundamental role in the dynamics of the vorticity field. It is bounded between 0 and 1. The final parameter, W^*, is also related to the vortex stretching mechanism. It is the cosine of the angle between the vortex stretching and

the vorticity vectors and indicates how efficient the vortex stretching mechanism is in stretching/compressing the vorticity field (note that the vortex stretching vector also changes the direction of the vorticity vector and this mechanism is taken into account in V^* but not in W^*). The parameter W^* is also bounded between -1 and 1, with positive values indicating vortex stretching and negative ones indicating vortex compression.

The boundedness of the parameters (6) is convenient not only for the data analysis performed in the next sections but also (and mainly) for future implementation in SGS models. The parameter Δ/z is special because in a simulation it would assume a finite number of discrete values determined by the filter width and the numerical grid. However, the local Richardson number (4) can vary continuously and is not bounded. To obtain a bounded parameter, the definition

$$\mathrm{Ri}^* = \mathrm{erf}(\mathrm{Ri}) \tag{7}$$

is used here, where erf is the error function and Ri* is bounded between -1 and 1.

In summary, the working hypothesis of this study is that the Smagorinsky model can be improved by allowing the coefficient to depend upon one or more of the six dimensionless parameters. Equation (2) becomes

$$c_s^2 = f(\Delta/z, \mathrm{Ri}^*, S^*, Q^*, V^*, W^*). \tag{8}$$

Note, however, that it is not possible to improve the alignment between the real and the modeled SGS stress tensor merely by changing the value of the coefficient. The best one can hope for is to improve the model's accuracy in representing the energy transfer to smaller scales.

b. Conditional averaging

When considering a functional relationship such as Eq. (8), the question being posed is, "for a prescribed set of parameter values (Δ/z, Ri*, S^*, Q^*, V^*, and W^*) what is the optimal value of the Smagorinsky coefficient?" An optimal value of the Smagorinsky coefficient is traditionally associated with the rate of dissipation of kinetic energy from the resolved to the unresolved range of scales. Specifically, as originally proposed for data analysis by Clark et al. (1979), the value of c_s^2 can be measured by requiring the Smagorinsky model to match the measured dissipation. The SGS dissipation is $-\tau_{ij}\tilde{S}_{ij}$, where τ_{ij} is the (SGS) stress tensor defined as

$$\tau_{ij} = \widetilde{u_i u_j} - \tilde{u}_i \tilde{u}_j, \tag{9}$$

and $\tilde{u}_i$ is the filtered (or resolved) velocity field. If we ask what the optimal value of the Smagorinsky coefficient is *given* that the set of parameters (Δ/z, Ri*, S^*, Q^*, V^*, and W^*) take on particular values, it is natural to evaluate the real and modeled averaged SGS dissipations, conditioned on these particular parameter values. Equating these (real and modeled) conditional SGS dissipations yields the value of c_s^2 as a function of the prescribed parameters according to

$$c_s^2(\Pi_1, \Pi_2, \ldots) = \frac{\langle -\tau_{ij}\tilde{S}_{ij} | \Pi_1, \Pi_2, \ldots \rangle}{\langle \Delta^2 |\tilde{\mathbf{S}}|^3 | \Pi_1, \Pi_2, \ldots \rangle}. \tag{10}$$

In Eq. (10), Π_1, Π_2, ... are dimensionless parameters such as Δ/z, Ri*, S^*, Q^*, V^*, and W^*. In practice, to determine $c_s^2(\Pi_1, \Pi_2, \ldots)$, each one of the allowable parameter ranges is divided in bins and the averages are computed within each bin.

At this stage, it is useful to add a few remarks about conditional averaging. Such averaging has been used before in the context of SGS modeling to address the challenges posed by the inherent variability and noisiness of the small scales of turbulence. Conditional averaging was used in analysis of experimental Particle Image Velocimetry data to find the conditional SGS force fields for particular features of the large-scale field, such as regions of large strain-rate magnitude (Meneveau and Katz 1999). As noted in several earlier works, such as in the context of optimal estimation theory (Adrian 1990; Langford and Moser 1999) and chaotic dynamics (Machiels 1997) given a fixed state of the large scales at a given time, it is expected that there exists an infinite number of possible subgrid-scale states. The best (optimal in order to reproduce the statistics and short-time behavior of the large-scale dynamics) among those is the "conditional average" with respect to the fixed state of the large scales. The conditional average should be done with respect to the entire large-scale field, as discussed in Langford and Moser (1999; see also Meneveau and Katz 2000). This is impossible to carry out in practice since the large scales are themselves a very high dimensional system. Thus in practice one must choose a dynamically significant subset of parameters, as we have done here. One may thus regard the conditionally averaged Smagorinsky coefficient as statistically the best choice given the parameters identified in the large scales. This choice will best reproduce the short-time evolution and probability density function (PDF) of the kinetic energy in the resolved field in LES given the knowledge (selected parameters) at hand about the large scales in the context of the Smagorinsky model. In this study, these arguments are applied in the context of ABL data.

3. Dataset and analysis procedures

The main dataset used here comes from the Horizontal Array Turbulence Study (HATS) field experiment, already extensively documented (Kleissl et al. 2003, 2004; Sullivan et al. 2003; Horst et al. 2004) and only briefly described here. The HATS field experiment took place in the San Joaquin Valley, California, in September 2000. Three setups of two horizontal arrays of three-dimensional sonic anemometers with different spacings were used to allow for different filter widths. The amount of data available and the geometric characteristics of both arrays are detailed in Table 1.

The data are divided into short runs of approximately 13.5 min, Taylor's hypothesis is used, and a horizontal rotation of the coordinate system is applied such that the x direction is aligned with the mean wind direction. Only runs in which the required rotation angle was smaller than 30° were used. The procedure for alignment is the same employed by Kleissl et al. (2003). The basic filter width is chosen to be $\Delta = 2\delta_y$ (δ_y is the horizontal distance between instruments in the lower array). A Gaussian filter is applied in the streamwise (x) direction and an approximated "top hat" filter in the lateral (y) direction. As in Horst et al. (2004), convolution with the top hat filter is evaluated by the trapezoidal integration rule. For $\Delta = 2\delta_y$, this is equivalent to weighted averages over 3 instruments. As shown by Kleissl et al. (2004), the use of three sonics instead of five [as thoroughly analyzed by Horst et al. (2004)] does not significantly affect the results. No filter is applied in the vertical direction. With the purpose of extending the Δ/z range, in section 4a, setups 1 and 2 are also filtered with $\Delta = 4\delta_y$ (in this case 5 instruments are used for filtering in the lateral direction).

Gradients of the filtered velocity field are approximated by finite differences. Second-order schemes are applied in x and y and first-order in z (for more detail see Tong et al. 1999; Porté-Agel et al. 2001b; Kleissl et al. 2003). From this dataset it is possible to measure the SGS stress tensor under different stability conditions and filter widths. For the filter width $\Delta = 2\delta_y$ (the one mostly used in this work), the array yields measured and modeled SGS stress at 5 lateral locations and results presented are averaged over them to improve statistical convergence.

Two secondary datasets are used to validate results obtained from HATS: a pseudospectral forced direct numerical simulation (DNS) of isotropic turbulence in a cubic box of size 2π using $(256)^3$ nodes with $\mathrm{Re}_\lambda = 128$, and random data with a Gaussian probability distribution function generated in the same grid as the DNS (this last dataset is modified using spectral rescaling to have a $-5/3$ power spectrum). These datasets are filtered with a 3D Gaussian filter with characteristic wavenumber $k_c = 8$, which corresponds to $\Delta_c/\eta \approx 35$ in the DNS (η is the Kolmogorov microscale). Derivatives are evaluated in Fourier space. In the DNS dataset there are no solid boundaries or buoyancy effects, and the main interest is to provide a comparison that validates the main results and extends them to a different (simpler) flow condition. The random data are used to determine whether a particular result has dynamic or kinematic origin (i.e., whether it is unique to fields obeying the Navier–Stokes equations or trivially valid for an arbitrary random vector field).

TABLE 1. Geometric description of arrays at the HATS field experiment. Here z is the height of the lower array, δ_y is the horizontal distance between instruments in the lower array, and δ_z is the vertical distance between arrays.

Array No.	Data (h)	z (m)	δ_y (m)	δ_z (m)	Δ (m)	Δ/z (–)
1	46.0	3.45	3.35	3.45	6.70	2.0
2	38.7	4.33	2.17	4.33	4.33	1.0
3	37.9	4.33	1.08	4.33	2.17	0.5

4. Results

a. Characterization of atmospheric stability

The first question to be addressed is whether the effects of atmospheric stability on the Smagorinsky coefficient presented in terms of average quantities by Kleissl et al. (2003) and Sullivan et al. (2003) can be described instead by the local stability parameter defined in Eq. (7). Figure 1a shows $c_s^2(\Delta/z, \mathrm{Ri}^*)$ calculated using Eq. (10) with $\Pi_1 = \Delta/z$ and $\Pi_2 = \mathrm{Ri}^*$ for the 3 arrays described in Table 1 as well as the version of arrays 1 and 2 filtered with width 2Δ. This figure clearly shows that the main effects of stability on c_s^2 are well described also in terms of the local Ri*. The significant decrease in the value of the coefficient for stable stratification is apparent, in accordance with Kleissl et al. (2003) and Sullivan et al. (2003). Note that although there are small differences between each curve, the general trend is very similar: there is a reasonable plateau with constant high values of c_s^2 for unstable cases and almost vanishing values for the strongly stable cases. The transition between these two clear regions is smooth and slightly different for different ratios Δ/z. The trend reported by Kleissl et al. (2003) of higher values associated with smaller Δ/z can also be clearly seen in this figure. These results support the notion that it is possible to characterize the effect of atmospheric stability on c_s^2 based on the local stability parameter as defined in Eq. (7).

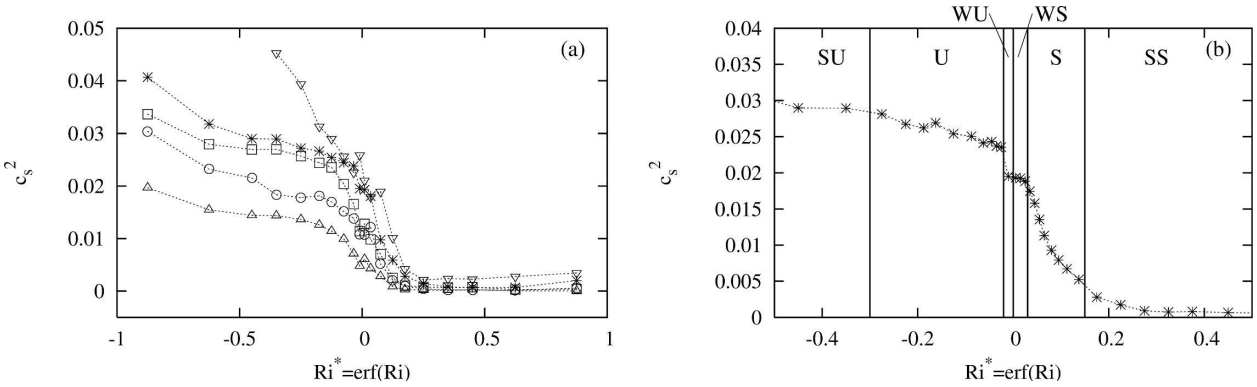

FIG. 1. (a) The Smagorinsky coefficient as a function of the local stability parameter for different Δ/z ratios—single filtered ▽: $\Delta/z = 0.5$; *: $\Delta/z = 1$; □: $\Delta/z = 2$; and double filtered ○: $\Delta/z = 2$; △: $\Delta/z = 4$. (b) Detail showing the division in stability categories for $\Delta/z = 1$. The categories are strongly unstable (SU), unstable (U), weakly unstable (WU), weakly stable (WS), stable (S), and strongly stable (SS).

In Fig. 1b, results for setup 2 (also used in the following sections) for a smaller range of Ri* and with smaller bins are shown. Based on this case, six stability categories are defined (Table 2). Results in the next sections are primarily averages within each of these categories.

b. *Atmospheric stability and resolved velocity gradient structure*

In this section, the influence of stability and distance from the surface on the resolved velocity gradient structure [characterized by the four dimensionless groups defined in Eq. (6)] is documented. The first reason for such analysis is to determine whether the invariants of the velocity gradient tensor are sensitive to changes in mean shear or distance from the ground and buoyancy. The second reason is that the importance of the effect of any parameter upon the average model is given by two factors: the effect on the coefficient itself and the probability distribution of the parameter. The approach consists of calculating PDFs of each parameter conditioned on Ri* and Δ/z. Figure 2 shows the PDFs for the 4 parameters corresponding to all 6 stability regimes and $\Delta/z = 1$. Also shown for comparison are the results for DNS and random data.

Figure 2a displays the PDFs for the local strain state S^*. As explicitly noted by Lund and Rogers (1994) and confirmed here, the PDF is flat for random data. The prevalence of axisymmetric extension ($S^* = 1$) found in turbulent flow fields by Lund and Rogers (1994) and Tao et al. (2002) is also confirmed for the DNS data and is clearly a dynamic feature of turbulence (i.e., not present in random data). The results for weakly unstable data also reproduce well the findings of Higgins et al. (2003) for a dataset under (globally) weakly unstable conditions. Although the shape of the PDF is very similar, clearly the peak is not as pronounced as for DNS. This difference may be due to a different Reynolds number, filter width, and/or effects of mean shear and buoyancy. The other curves presented in Fig. 2a clearly show the differences of the structure of the flow under stable and strongly stable conditions, when the peak moves from axisymmetric extension to plane shear at $S^* = 0$. The reason for this change is that under very stable conditions the turbulence is strongly suppressed and even locally the flow is dominated by the mean shear (note that $S^* = 0$ is the strain state of the mean flow).

The PDFs of W^* are shown in Fig. 2b, characterizing the distribution of alignment between the vortex stretching and the vorticity vectors. The curves for DNS and random data are similar to those presented by Shtilman et al. (1993), who noted that the alignment between these vectors is also a dynamic characteristic of turbulence, and its asymmetry is associated with positive enstrophy generation. Once again the peaks are less pronounced in the HATS dataset. Note that, like S^*, all the PDFs of W^* are very similar and the main differences appear for the strongly stable curve, where the PDF displays a slight predominance of negative values. This is associated with a smaller or even negative resolved enstrophy production under stable conditions.

TABLE 2. Stability categories as defined from Fig. 1b.

Category	Ri*
Strongly unstable (SU)	$-1 \le \text{Ri}^* < -0.3$
Unstable (U)	$-0.3 \le \text{Ri}^* < -0.02$
Weakly unstable (WU)	$-0.02 \le \text{Ri}^* < 0$
Weakly stable (WS)	$0 \le \text{Ri}^* < 0.03$
Stable (S)	$0.03 \le \text{Ri}^* < 0.15$
Strongly stable (SS)	$0.15 \le \text{Ri}^* \le 1$

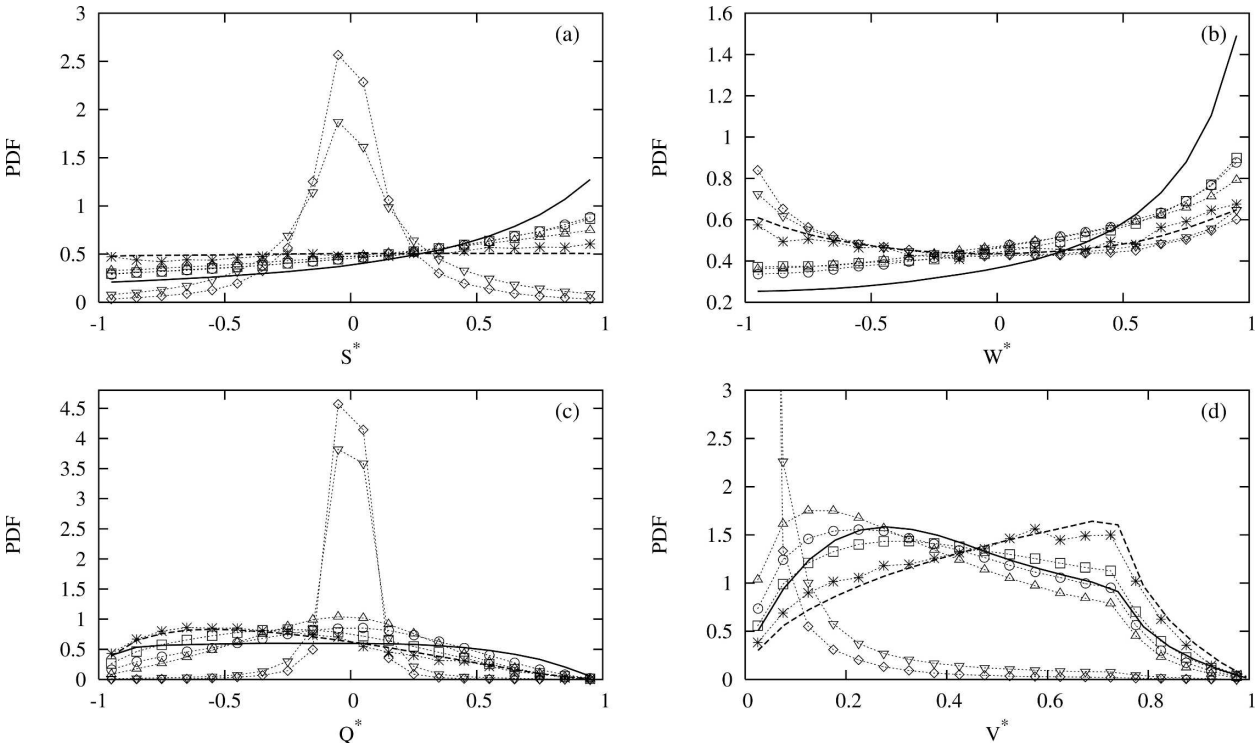

FIG. 2. PDF of (a) S^*, (b) W^*, (c) Q^*, and (d) V^* conditioned on atmospheric stability; *: strongly unstable; □: unstable; ○: weakly unstable; △: weakly stable; ▽: stable; ◇: strongly stable; —: neutral DNS; and - -: random data.

At this point we are not able to explain the observation of negative net enstrophy production under strongly stable conditions.

The PDFs for Q^* presented in Fig. 2c also have some interesting features because they contain information about relative magnitudes of vorticity and strain rate. However, these results must be examined carefully, since the PDF for random data itself has a pronounced trend toward strain-dominated regions. All other curves should then be compared to the one for random data. For stable datasets there is a strong shift of the peak of the PDFs to $Q^* = 0$, corresponding to homogeneous shear, again the state of the mean flow (note that for the mean flow one has $|\tilde{\mathbf{S}}|^2 = |\tilde{\boldsymbol{\omega}}|^2$ and so $Q^* = 0$). In addition, the more unstable the dataset, the more frequent strain-dominated regions appear (note that the PDFs for unstable data peak in the negative region of Q^* and those for stable cases do not). As one moves to less unstable and then stable local conditions, more regions dominated by vorticity are encountered. The DNS data show a similar behavior in that they are above the random data for $Q^* > 0$ and below them for $Q^* < 0$.

The PDF for V^* is shown in Fig. 2d. Again the PDF for random data is not flat. However, it is clear that under unstable conditions, events with strong vortex stretching become more frequent. This is also an expected result, since more stable conditions imply smaller turbulent intensities and the statistics are dominated by the two dimensional laminar flow where no vortex stretching exists.

On the PDFs of S^*, Q^*, and V^*, the key feature is the effect of the mean flow (W^* is not defined for the mean flow, since both its numerator and denominator vanish). The shape of the PDF will be determined by the relative importance of the mean flow and the resolved turbulence. Whenever the resolved turbulence dominates, the PDFs are similar to those for the strongly unstable conditions, meaning that axisymmetric extension prevails in the PDF of S^* and the PDFs of Q^* and V^* are similar to those for random data (see strongly unstable cases in Fig. 2). On the other hand, when the mean velocity gradient is dominant, the PDFs peak at the mean flow state ($S^* = 0$, $Q^* = 0$, and $V^* = 0$). Whether the resolved turbulence is able to overcome the effect of the mean flow and dominate the statistics of the invariants is determined by the amount of resolved turbulence, and consequently by the relation between the filter width and the integral scale of the turbulence. Recall also that the integral scale in the atmospheric boundary layer is related to the distance from the surface and the atmospheric stability. To further

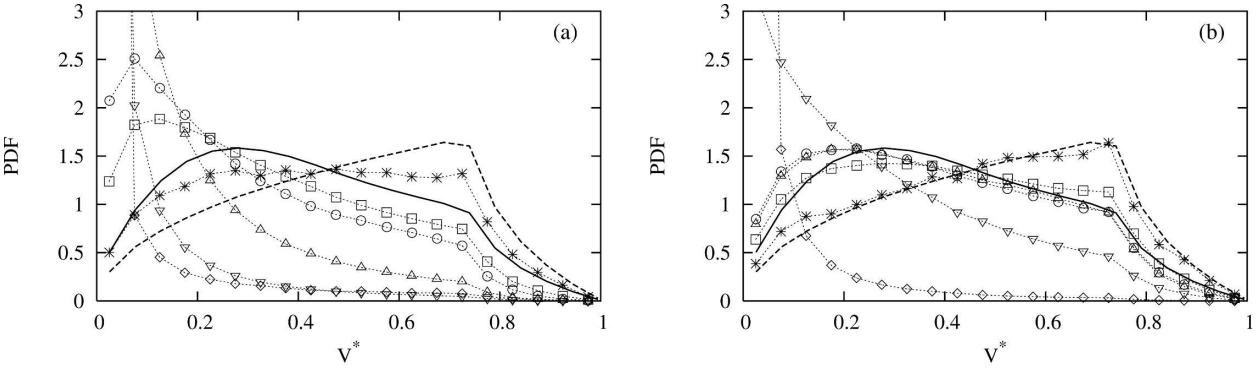

FIG. 3. PDF of V^* for (a) setup 1 ($\Delta/z = 2$) and (b) setup 3 ($\Delta/z = 0.5$) conditioned on atmospheric stability. For legend see Fig. 2.

investigate this issue the PDFs of V^* for setups 1 and 3 are shown in Fig. 3. Here V^* is chosen instead of S^* or Q^* because the effects are more evident.

Comparison between the PDFs of V^* for the three setups makes evident the combined effects of Ri* and Δ/z. The PDFs for the strongly stable case are dominated by the mean flow independently of Δ/z (see Figs. 2d and 3a,b). It is interesting to compare the strongly stable with the weakly stable regime. In the weakly stable case, the resolved turbulence is strong enough to overcome the mean shear for the well-resolved field (i.e., $\Delta/z = 0.5$ in Fig. 3b). However, as one decreases the resolution by increasing the value of Δ/z (Figs. 2d and then 3a), less turbulence is resolved and the PDF moves toward the strongly stable limit. It is also clear in Fig. 3a that even the strongly unstable case, when filtered at a large scale as compared to the integral scale, is dominated by the mean shear.

The results presented in this section clearly show the effects of atmospheric stability and distance from the ground on the structure of the resolved velocity gradient tensor. Most of these effects originate from the relative importance between the resolved turbulence and the mean flow, a factor that changes with stability, distance from the ground, and filter width. To confirm this interpretation of the trends, all the analyses presented here were repeated removing the mean flow (not shown). Indeed, the pronounced peaks for the strongly stable cases at $S^* = 0$, $Q^* = 0$, and $V^* = 0$ nearly disappear. However, we stress that removing the mean flow is not a practical approach in LES of highly nonstationary and inhomogeneous ABL flows.

These results support the hypothesis that the local structure of the resolved turbulent flow field is sensitive to effects of mean shear, buoyancy, and proximity to the ground, and that the local parameters defined in section 2 can be used to characterize, at least in part, these processes.

c. *Effects on SGS dissipation*

Before proceeding and analyzing the results for the Smagorinsky coefficient, a comment is needed on the conditional averages of the SGS dissipation [i.e., the numerator of Eq. (10)]. From the high correlation between the SGS dissipation and the invariants I_2 and I_5 in isotropic turbulence (Borue and Orszag 1998), one would expect both S^* and W^* to have a significant impact on the measured dissipation. Figure 4a shows

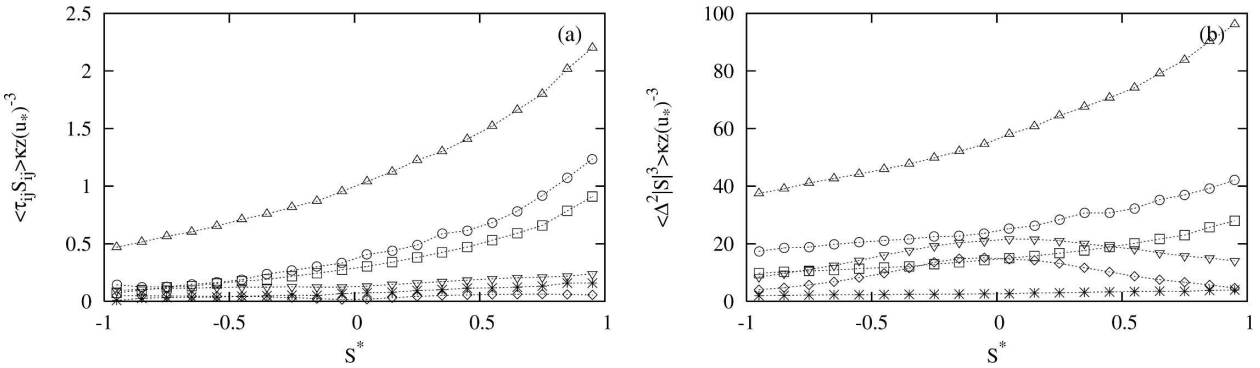

FIG. 4. Dependence of (a) SGS dissipation and (b) Smagorinsky dissipation on S^*. For legend see Fig. 2.

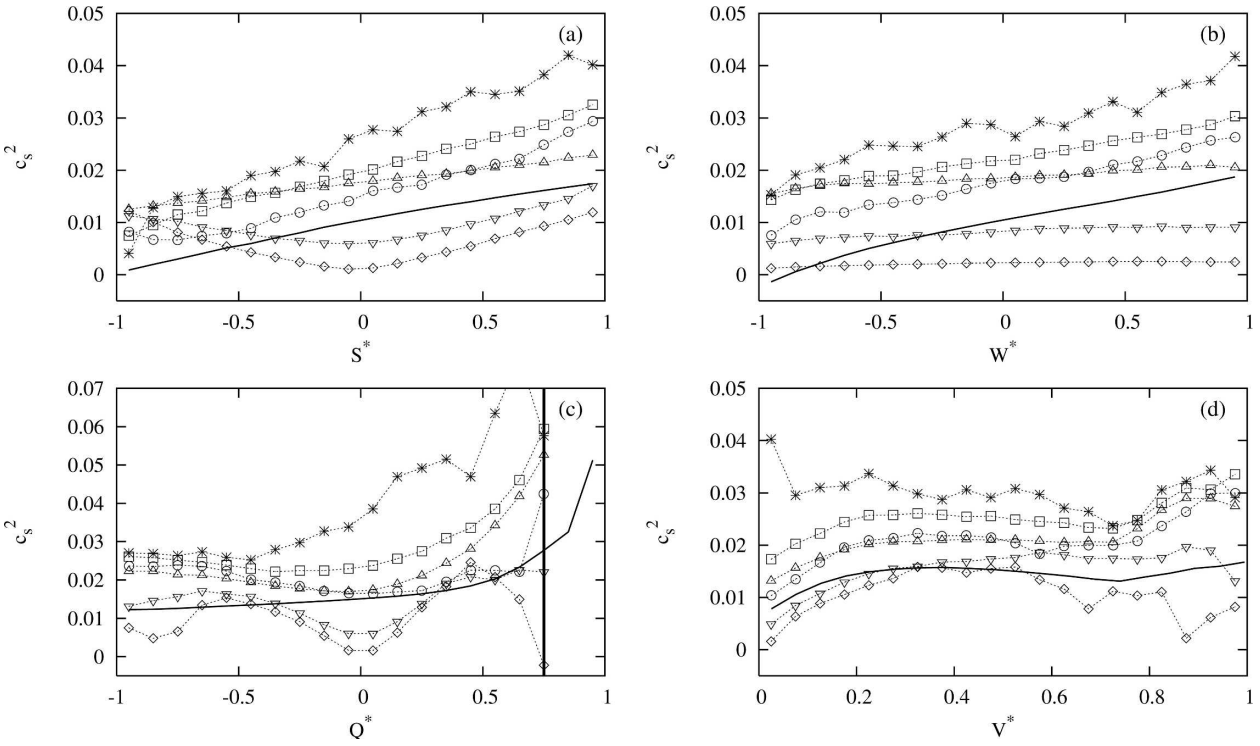

FIG. 5. Dependence of c_s^2 on (a) S^*, (b) W^*, (c) Q^*, and (d) V^* for each atmospheric stability regime. For legend see Fig. 2.

the SGS dissipation conditionally averaged on Ri* and S^* for $\Delta/z = 1$. All curves are made dimensionless by the inertial range scaling for dissipation $\kappa z/u_*^3$, where u_* is the average friction velocity. As expected, regions of high SGS dissipation are associated with positive values of S^* (except for the strongly stable case that displays a minimum at $S^* = 0$). The dissipation modeled by the Smagorinsky model (without the coefficient c_s^2) is shown in Fig. 4b and displays the same qualitative behavior as the measured SGS dissipation except for the stable and strongly stable cases. In these two cases the spurious effects of the mean flow on the Smagorinsky model result in an eddy viscosity that is too high. Clearly these effects are predominant in regions where the mean flow is stronger and $S^* \approx 0$. Since the optimal value of the Smagorinsky coefficient is determined by the ratio between the quantities in Figs. 4a,b [see Eq. (10)], the differences between modeled and measured SGS dissipation cannot be described by a constant value for c_s^2.

Similar analyses were performed for the other parameters (not shown). As expected, high SGS dissipation is associated with positive values of W^* (vortex stretching) and negative values of Q^* (this is also expected because it is well known that dissipation occurs primarily in regions of high strain, as opposed to regions of high rotation). Again the exception is the strongly stable case, for which the peak moves toward $Q^* = 0$. There is no clear trend of the dissipation with V^*. Therefore one can conclude that the SGS energy transfer is affected by the alignment between vorticity and vortex stretching vectors, rather than the magnitude of the vortex stretching vector itself. The general form of these trends is qualitatively well predicted by the Smagorinsky model, except when the mean flow dominates the resolved turbulence.

d. Effects on Smagorinsky coefficient

In this subsection, the additional impact of local flow parameters on the optimal value of the Smagorinsky coefficient is documented (i.e., the dependence of c_s^2 on S^*, Q^*, V^*, and W^*). For simplicity it is convenient to begin by analyzing each parameter independently, which requires calculating $c_s^2(\Delta/z, \text{Ri}^*, \Pi)$ using Eq. (10) where Π is any of the four parameters describing the local structure of the velocity gradients.

Figure 5 shows the dependence of c_s^2 on each parameter (all results for setup 2 and $\Delta/z = 1$). The effect of S^* on c_s^2 is presented in Fig. 5a. It is clear that not only the strain state has an important effect on the value of c_s^2 but also that this effect changes with atmospheric stability. All the unstable regimes present a similar linear dependence, displaying an offset to higher values as the flow becomes more unstable. The weakly stable

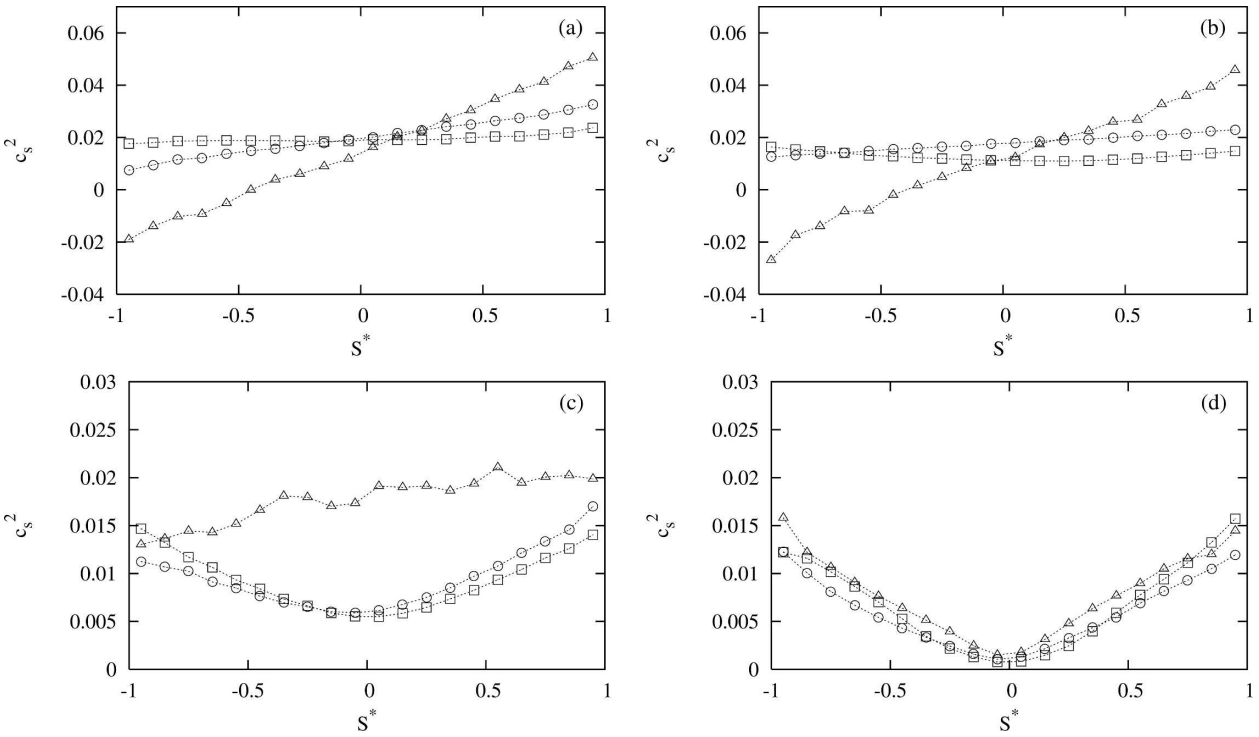

FIG. 6. Dependence of c_s^2 on S^* for all three setups for (a) unstable, (b) weakly stable, (c) stable, and (d) strongly stable regimes; □: setup 1 ($\Delta/z = 2$); ○: setup 2 ($\Delta/z = 1$); and △: setup 3 ($\Delta/z = 0.5$).

case is still not very different from the unstable ones. Once again, the main difference is the stable and strongly stable cases that have a strong minimum at $S^* = 0$. This is another consequence of the important effect of mean shear under these conditions and was expected based on the results from the previous section. Since the mean flow does not affect $\boldsymbol{\tau}$ (note that no filtering is done in the vertical direction) but does affect $\tilde{\mathbf{S}}$, its effect is stronger on the denominator of Eq. (10) than on its numerator, causing c_s^2 to decrease. Thus, under very stable conditions, in regions where turbulence is weak and the flow is mostly dominated by the mean shear, c_s^2 decreases. Note in Fig. 2a that $S^* = 0$ is exactly the peak in the PDF of S^* for this stability. The peak of the PDF at $S^* = 0$ and the low value of c_s^2 for this state lead to the decrease in c_s^2 under stable conditions (see Fig. 1). However, setting the coefficient to its mean value everywhere under stable conditions would be underdissipative in the regions where $S^* \neq 0$.

The effect of W^* on the Smagorinsky coefficient is shown in Fig. 5b. The general trends are very similar to those obtained for S^*, although slightly weaker. There is also a small difference in the strongly stable case, where the minimum found at $S^* = 0$ is not present at $W^* = 0$. Note that for all parameters analyzed here, the only region where c_s^2 becomes negative for the DNS data is for $W^* \approx -1$. This is a sign that the energy backscatter is associated with regions of strong vortex compression. This result is physically sound, since one may imagine that the compression of vortex filaments generates larger structures and the energy contained by the filaments is then associated with larger scales. No negative values of c_s^2 are found for the HATS data in Fig. 5b and this issue will be further discussed with Fig. 6. The fact that the Smagorinsky model is fully dissipative, not allowing the backscatter of energy, has been regarded as a deficiency in the model (Leith 1990; Mason and Thomson 1992) but is an advantage from the point of view of numerical stability and robustness.

Figure 5c shows the effect of Q^* on c_s^2. The results for DNS have a clear trend of increasing coefficients for regions of stronger vorticity. As Q^* approaches 1, the SGS dissipation goes to zero. The dissipation modeled by the Smagorinsky closure also goes to zero, but too fast. This is the cause for the increase in the value of c_s^2. Beyond $Q^* = 0.75$, both dissipations are very small and the value of the coefficient grows too large and is susceptible to errors (for this reason it is not plotted for the HATS dataset). Figure 5d contains the analysis for V^*. In this case the trends are not strong.

These analyses were repeated for setups 1 and 3 to determine the effect of Δ/z on the results described so

far. The general form of the dependence does not change much, but the dependence on both S^* and W^* becomes more pronounced as Δ/z decreases while the dependence on Q^* and V^* does not. The effect of Δ/z on S^* for different stability conditions is illustrated in Fig. 6. Figure 6a is the case for unstable data and is representative of any local unstable condition. For the largest ratio $\Delta/z = 2$ the dependence is very weak, and it becomes stronger as the ratio is decreased. Although the dataset used does not allow for smaller ratios, one expects that farther from the ground (i.e., for small enough ratios of Δ/z) the trend becomes independent of Δ/z. More negative values of the coefficient are found as Δ/z decreases, consistent with the results of Sullivan et al. (2003), who noticed stronger backscatter when the turbulence is better resolved. Figures 6a,b also show the clear association of backscatter (negative values of c_s^2) with negative values of S^*. Backscatter is also associated with negative values of W^* (not shown) and this relation will be explained in the discussion about the joint PDFs of S^* and W^* (following Fig. 8).

Figures 6b,c for the weakly stable and the stable regimes help illustrate the relation between the resolved turbulence and the effects of mean flow. It is clear that for weakly stable cases, if enough energy is resolved, turbulence dominates the statistics and the trend of c_s^2 is similar to the one for unstable cases (e.g., $\Delta/z = 1$ and $\Delta/z = 0.5$ in Fig. 6b). However, if the filter is large and the resolved turbulence is not strong compared to the mean shear, the trends are similar to those for the strongly stable case (e.g., $\Delta/z = 2$ in Fig. 6b). The same effect is seen for the well-resolved stable case in Fig. 6c. Once again, in the strongly stable case (Fig. 6d) the turbulence is so weak that even for the well-resolved case the mean shear dominates and there is no Δ/z dependence on the curves for c_s^2. The effects of Δ/z on the trends for W^* are similar to those presented here for S^* and there is almost no effect on Q^* and V^* (not shown).

Although this issue is not analyzed here, part of this dependence of c_s^2 originates from the misalignment between $\tilde{\mathbf{S}}$ and $\boldsymbol{\tau}$. It is well known that when the SGS stress tensor is decomposed into Leonard, cross, and Reynolds contributions (see Germano 1986), some of the alignment properties are characteristic of the Leonard term only (Tao et al. 2002; Higgins et al. 2003). To determine whether the results reported so far originate from the Leonard term only, each term is calculated using the Germano decomposition: the Leonard term given by $\mathcal{L}_{ij} = \widetilde{\tilde{u}_i\tilde{u}_j} - \tilde{\tilde{u}}_i\tilde{\tilde{u}}_j$, the cross term given by $C_{ij} = \widetilde{\tilde{u}_iu_j'} + \widetilde{u_i'\tilde{u}_j} - \tilde{\tilde{u}}_i\tilde{u}_j' - \tilde{u}_i'\tilde{\tilde{u}}_j$, and the Reynolds term given by $\mathcal{R}_{ij} = \widetilde{u_i'u_j'} - \tilde{u}_i'\tilde{u}_j'$. In the last two expressions, u_i' is the subgrid velocity obtained by subtracting the resolved part from the full velocity field. The same procedure of calculating conditional averaged values of c_s^2 is repeated, using first $\mathcal{L}_{ij}$ and then $(C_{ij} + \mathcal{R}_{ij})$ instead of τ_{ij} in Eq. (10). The first part, $(c_s^2)^L$, represents the contribution of the Leonard term to the dependence found for the Smagorinsky coefficient, and the second one, $(c_s^2)^R$, is the remainder contribution. In this way, the coefficient is decomposed into $c_s^2 = (c_s^2)^L + (c_s^2)^R$, and effects from the trivial Leonard part can be isolated. Figure 7 shows this decomposition as a function of S^* for different atmospheric stabilities and $\Delta/z = 1$. As expected, since the filter width and the integral scale are of the same order, the contribution from the Leonard term is small. Figure 7a shows the comparisons for the unstable case, which is very similar to the strongly and weakly unstable cases (not shown). The dependence of the Leonard part on S^* is stronger, but the remainder part also contributes to the total result. Data for the weakly unstable case shown in Fig. 7b are also similar to the unstable cases. For the stable and strongly stable cases shown in Figs. 7c,d, the contributions from the Leonard term are almost negligible and the trends are mostly determined by the remainder part. However, the Leonard part still presents trends qualitatively similar to the remainder. Decomposition for the other parameters is similar and is not shown here. The results suggest that most of the observations made here for the Smagorinsky model could also be useful for mixed models [i.e., any of the many variants of the mixed model originally proposed by Bardina et al. (1980)].

With this knowledge of the role played by each individual parameter, the next step is to combine them and determine their joint PDFs and the values of c_s^2 (Δ/z, Ri*, S^*, Q^*, V^*, W^*). At the present stage, the amount of data required to ensure converged statistics in each bin in the six-dimensional space is impractical. Instead we apply a more practical approach, selecting the two most relevant out of the four velocity gradient parameters. We select S^* and W^* because they have already been directly associated with the energy transfer mechanisms in the literature (Borue and Orszag 1998), they present nearly evenly distributed PDFs (meaning that all states occur with a reasonable frequency), and they also have a strong effect upon the value of c_s^2 (see Figs. 5a,b). Although the dependence on W^* is not as strong in Fig. 5b, it is much stronger for setup 3 ($\Delta/z = 0.5$). The other possible choice would be Q^* instead of W^*. However, most of the influence of Q^* on the coefficient occurs in its positive range, where the number of points is not large and the dissipation is usually low.

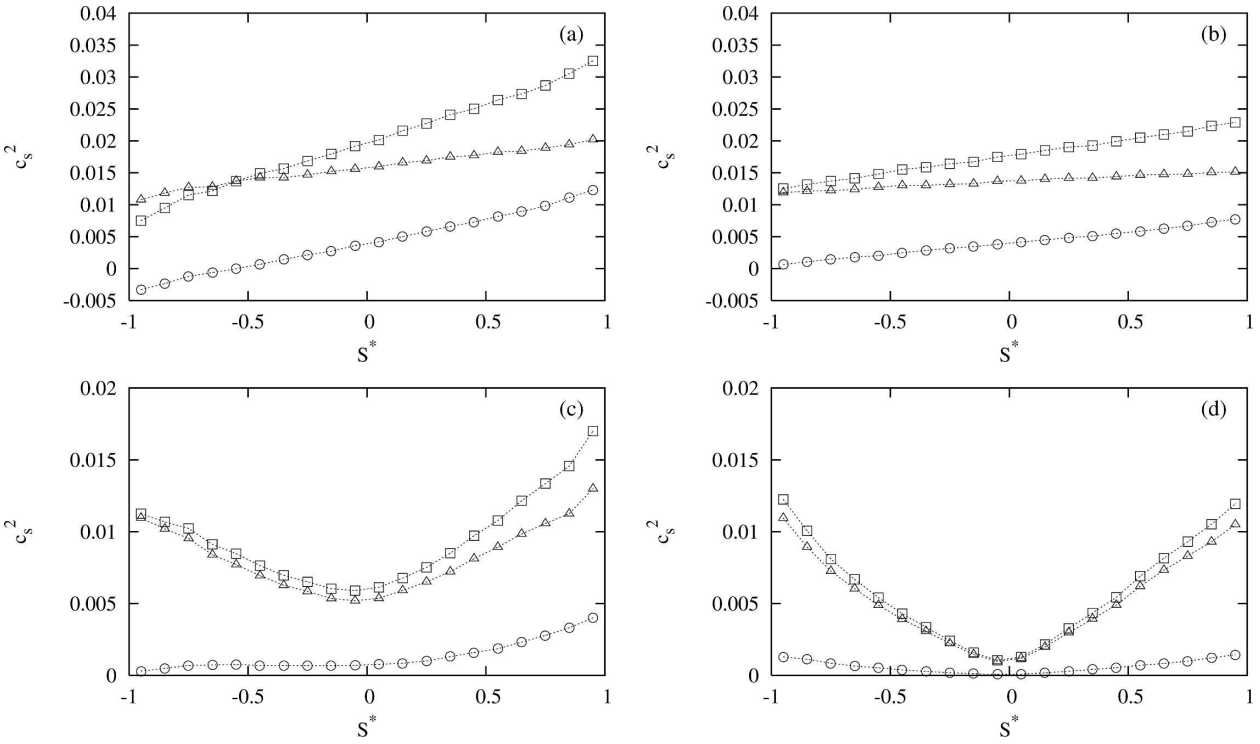

FIG. 7. Decomposition into Leonard and remainder contributions to c_s^2 against S^* for (a) unstable, (b) weakly stable, (c) stable, and (d) strongly stable regimes; □: c_s^2; ○: $(c_s^2)^L$; and △: $(c_s^2)^R$.

Therefore, in what follows, the joint PDFs of S^* and W^* and the behavior of the coefficient c_s^2 (Δ/z, Ri*, S^*, W^*) are studied.

Figure 8 displays the changes of the joint PDFs of S^* and W^* as the atmospheric condition changes from strongly unstable to strongly stable stratification. Most of the points are concentrated around the diagonal $W^* = S^*$. This is a kinematic artifact since it is reproduced in random data as well (shown in Fig. 9). However, the PDF for random data shows a significant probability in the entire plane and is antisymmetric with relation to the axis $S^* = 0$, meaning that both extrema ($S^* = W^* = 1$ and $S^* = W^* = -1$) are equally probable. The dynamic feature of turbulence is manifested in the strong predominance of the $S^* = W^* = 1$ state in the data. For the strongly unstable case, the peak at $S^* = W^* = 1$ is clear, but a significant level of probability density also exists at other values (although still lower than for the random data). As one moves toward less unstable data, the distributed probability decreases and most of the points concentrate around the main curve. The DNS result (not shown) is very similar to the weakly unstable case, although with a more pronounced peak. As one keeps moving toward weakly stable and then stable cases, the strength of the peak decreases as the entire curve becomes more equally distributed. The strongly stable case is very different; there is a strong concentration around $S^* = 0$ but an almost even distribution along the entire range of W^*.

The relation between S^* and W^* has a simple explanation. For incompressible flows, S^* has the sign of the intermediate eigenvalue of $\tilde{\mathbf{S}}$. It is well known that the vorticity vector is preferentially aligned with the intermediate eigendirection (Ashurst et al. 1987; Tao et al. 2002; Higgins et al. 2003). As a consequence, when the intermediate eigenvalue is negative (i.e., $S^* < 0$), the vorticity will more likely be in a compressing direction and $W^* < 0$. Similarly, for a positive intermediate eigenvalue (i.e., $S^* > 0$), the vorticity will more likely be in a stretching direction and $W^* > 0$.

The simultaneous dependence of c_s^2 on S^* and W^* is presented in Fig. 10 for all six stability regimes. As can be seen in Fig. 8, most of the S^*–W^* plane has a low density of points. To provide reliable statistics, larger bins were used to capture the joint dependence and results were interpolated to generate the smooth variations shown in Fig. 10. The progressive changes in the values of c_s^2 from the strongly unstable to the strongly stable cases are clear. The average value of the coefficient decreases and its distribution on the plane also changes considerably. As the atmosphere becomes

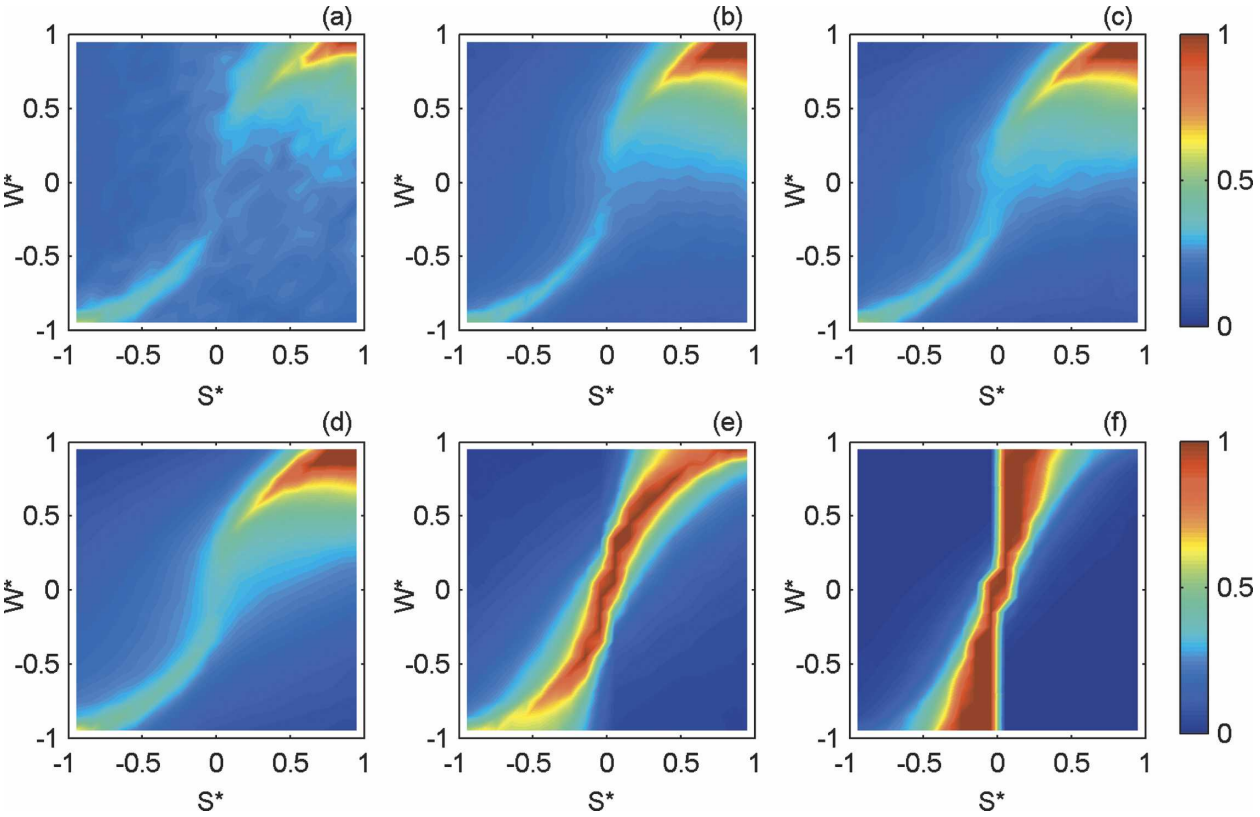

FIG. 8. Joint PDFs of S^* and W^* for each atmospheric stability regime: (a) strongly unstable, (b) unstable, (c) weakly unstable, (d) weakly stable, (e) stable, and (f) strongly stable.

more stable the effects of mean shear become stronger. This can be identified in the figure by the marked low values of the coefficient in the regions dominated by the mean flow (i.e., near $S^* = 0$) for the stable regimes. It is clear that if both parameters are taken into account instead of only one, a better representation of the measured dissipation can be achieved.

e. *Factorization of joint dependence*

The results presented so far provide evidence for the complex behavior of the Smagorinsky coefficient when more than one parameter is considered. An important question is whether the observed joint dependence could be factored, that is, if it can be written as the product of functions that depend individually on the parameters [as was proposed, e.g., in the functional form of Eq. (14) in Kleissl et al. (2003)]. In general, one would like to assess whether, for example, a dependence $c_s^2 = f(\Pi_1, \Pi_2)$ can be factorized as $c_s^2 = f_1(\Pi_1) f_2(\Pi_2)$. A convenient method to elucidate the possibility of such a factorization is to take the logarithm of the measured joint function and evaluate partial derivatives. Specifically, we evaluate

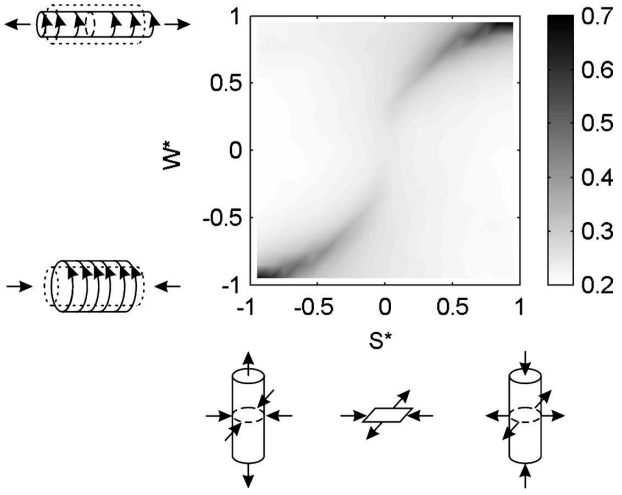

FIG. 9. Joint PDFs of S^* and W^* for random data. Also illustrated are three types of flow deformation [axisymmetric contraction ($S^* = -1$), plane shear ($S^* = 0$), and axisymmetric extension ($S^* = 1$)] and the vortex compression ($W^* = -1$) and vortex stretching ($W^* = 1$) mechanisms.

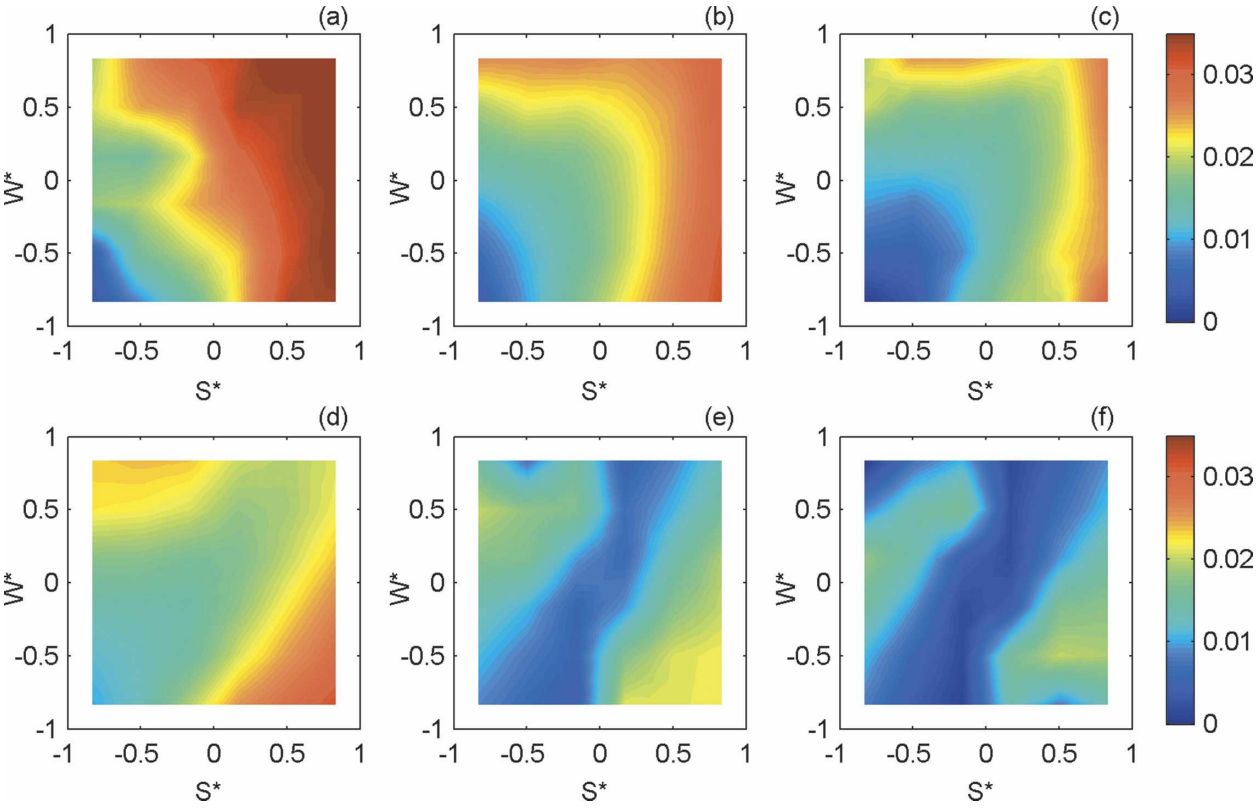

FIG. 10. The joint dependence of c_s^2 on S^* and W^* for each atmospheric stability regime: (a) strongly unstable, (b) unstable, (c) weakly unstable, (d) weakly stable, (e) stable, and (f) strongly stable.

$$\frac{\partial}{\partial \Pi_1} \log[f(\Pi_1, \Pi_2)] = g_1(\Pi_1, \Pi_2)$$

$$\frac{\partial}{\partial \Pi_2} \log[f(\Pi_1, \Pi_2)] = g_2(\Pi_1, \Pi_2). \quad (11)$$

If the factorization is possible, g_k (Π_1, Π_2) is only a function of Π_k. As an example, we consider the joint dependence of c_s^2 on Ri* and S^*. This joint dependence is measured from the data using additional bins for Ri*, and results are shown in Fig. 11a. The goal is to determine whether the joint dependence can be factorized as $c_s^2(\text{Ri}^*, S^*) = f_1(\text{Ri}^*) f_2(S^*)$. In Figs. 11b,c, the derivatives with respect to Ri* and S^* of the logarithm of $c_s^2(\text{Ri}^*, S^*)$ are shown. If the factorization is possible, the functions in Figs. 11b,c should depend only on Ri* and S^*, respectively. Although most of the dependence in Fig. 11b is actually on Ri* (partially supporting the possibility of factorization), Fig. 11c is clearly not a function only of S^*. The conclusion is that $c_s^2(\text{Ri}^*, S^*)$ cannot be properly represented by the product $f_1(\text{Ri}^*)$ f_2 (S^*).

It is also of interest to determine whether for a given stability range, the joint dependence on S^* and W^* (i.e., Fig. 10) can be factorized. Three illustrative cases are shown in Fig. 12. Figures 12a–c are the derivatives with respect to S^* for the unstable, weakly stable, and stable cases and Figs. 12d–f are the derivatives with respect to W^* for the same stabilities. For the factorization to be possible, the fields in Figs. 12a–c should be functions only of S^* and in Figs. 12d–f only of W^*. This is clearly not the case. The same conclusion holds for the other three stability regimes not shown here.

5. Discussion

In this work several locally defined dimensionless parameters have been introduced and used to characterize important local mechanisms of turbulent ABL flows. A priori analysis of data measured in the atmospheric surface layer and direct numerical simulation of isotropic turbulence have been used to show that these parameters have a marked impact upon the optimal value of the Smagorinsky coefficient.

Results presented here clearly show that the local Richardson number is efficient in capturing the effects of local atmospheric stability upon the value of the

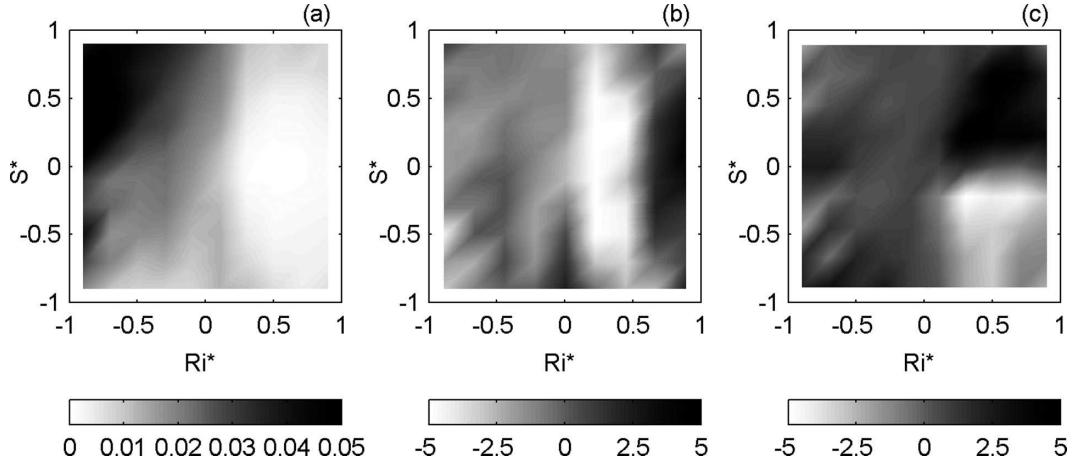

FIG. 11. The (a) joint dependence of c_s^2 on (Ri*, S*), and the partial derivatives of its logarithm with respect to (b) Ri* and (c) S*.

Smagorinsky coefficient. This is an important result because previous parameters used to characterize such effects are defined based on average quantities and require strong assumptions, such as homogeneity and/or stationarity. In addition, the ratio between filter width and distance from the surface was used to characterize the influence of the ground surface. The Richardson number and distance from the ground characterize the

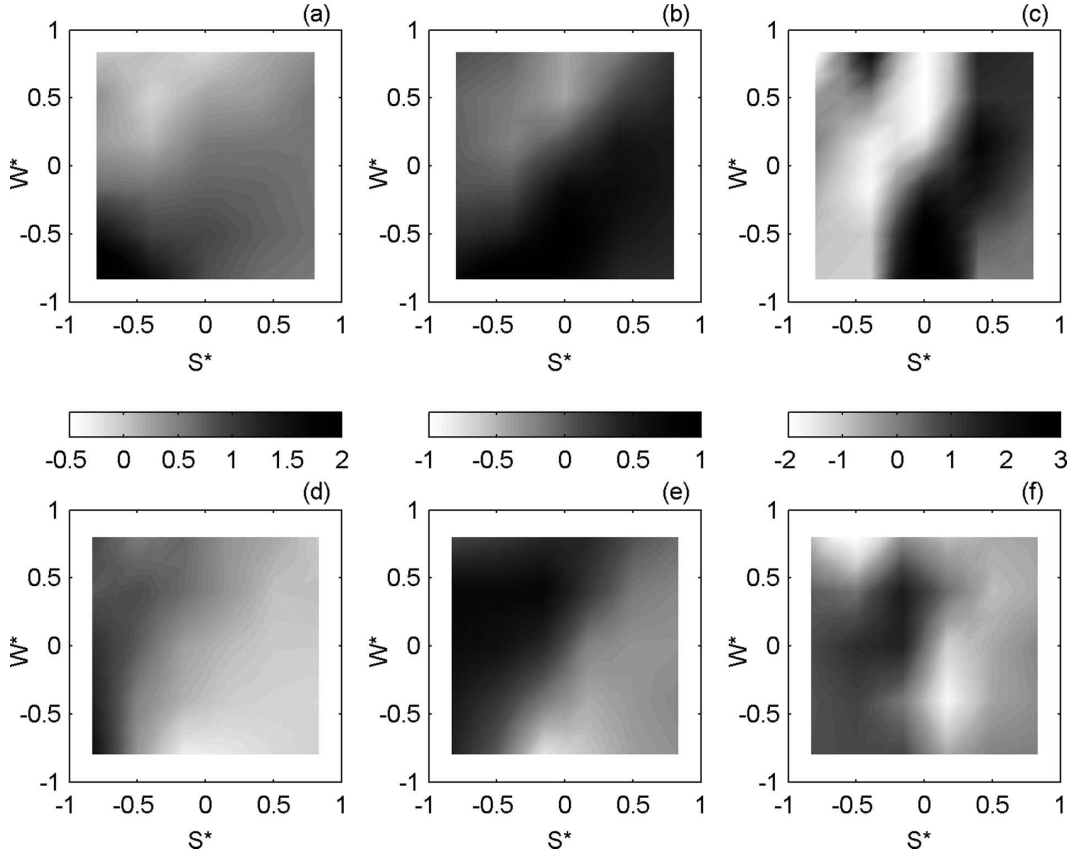

FIG. 12. Partial derivatives of $\log[c_s^2(S^*, W^*)]$ with respect to (a) S* for unstable, (b) S* for weakly stable, (c) S* for stable, (d) W* for unstable, (e) W* for weakly stable, and (f) W* for stable data.

integral scale of the turbulence, and by introducing the filter width one obtains a good description of how much of the turbulence is resolved.

To further characterize the influence of the local structure of the resolved turbulent field on the Smagorinsky coefficient, a set of dimensionless parameters based on the invariants of the velocity gradient tensor were defined. These parameters measure local properties such as strain state, balance between vorticity and strain, and relative magnitude of vortex stretching and its efficiency in changing the enstrophy. Probability density functions were used to study how the atmospheric stability affects the structure of the resolved velocity gradient tensor. Results show that the shape of the PDFs is mostly determined by the relative importance of the mean shear and the resolved turbulence. Under strongly stable stratification, the resolved turbulence is not able to dominate over the effect of the mean shear, identified by the peaks at $S^* = 0$, $Q^* = 0$, and $V^* = 0$. For the other stable regimes, the position of the peak depends on the amount of resolved turbulence (i.e., the relation between integral scale and filter width).

By requiring the Smagorinsky model to match the measured SGS dissipation on a conditional average sense, the dependence of the optimal values for the coefficient upon the four parameters used to characterize the local structure of the turbulent flow field is determined. When compared to the values usually employed in LES, the dependence found is actually quite strong. Most of the discussion has centered on comparing the resulting values to the theoretical value determined by Lilly (1967) ($c_s \approx 0.17$ or $c_s^2 = 0.03$) and the empirical one used by Deardorff (1970) ($c_s = 0.1$ or $c_s^2 = 0.01$). As can be seen in the results presented here, the optimal values exceed this range in both directions depending on the local structure of the resolved turbulent field.

The results suggest that one can improve the performance of the Smagorinsky model in predicting the SGS dissipation by including the dependence of the coefficient on dimensionless parameters to characterize the local structure of the turbulence. The agreement between many of the results obtained for the DNS of isotropic turbulence and the complex atmospheric data (where mean shear and buoyancy coexist) suggests that these trends are quite robust. However, the joint dependence was shown to require functional descriptions that are not amenable to factorization. This complicates the task of parameterization when many parameters are involved. Nevertheless, these results may be useful in reformulating the dynamic model based on conditional averaging rather than averaging over homogeneous directions (Germano et al. 1991) or over Lagrangian time histories (Meneveau et al. 1996). Such proposed new dynamic models will be the focus of future work.

Acknowledgments. This work was supported by National Science Foundation Grant ATM-0222238. The authors also acknowledge partial support of the Fonds National Suisse (200021-107910).

REFERENCES

Adrian, R. J., 1990: Stochastic estimation of sub-grid scale motions. *Appl. Mech. Rev.,* **43,** 214–218.

Ashurst, W. T., A. R. Kerstein, R. M. Kerr, and C. H. Gibson, 1987: Alignment of vorticity and scalar gradient with strain rate in simulated Navier-Stokes turbulence. *Phys. Fluids,* **30,** 2343–2353.

Bardina, J., J. H. Ferziger, and W. C. Reynolds, 1980: Improved subgrid scale models for large eddy simulation. American Institute of Aeronautics and Astronautics Paper 80-1357, 10 pp.

Borue, V., and S. A. Orszag, 1998: Local energy flux and subgrid-scale statistics in three-dimensional turbulence. *J. Fluid Mech.,* **366,** 1–31.

Boussinesq, J., 1877: Essai sur la théorie des eaux courantes. *Mém. prés. par div. savants à l'Acad. Sci.,* **23,** 1–680.

Bou-Zeid, E., C. Meneveau, and M. Parlange, 2005: A scale-dependent Lagrangian dynamic model for large eddy simulation of complex turbulent flows. *Phys. Fluids,* **17,** 025105, doi:10.1063/1.1839152.

Canuto, V. M., and Y. Cheng, 1997: Determination of the Smagorinsky–Lilly constant C_s. *Phys. Fluids,* **9,** 1368–1378.

Carper, M. A., and F. Porté-Agel, 2004: The role of coherent structures in subfilter-scale dissipation of turbulence measured in the atmospheric surface layer. *J. Turbulence,* **5,** 1–24.

Chong, M. S., A. E. Perry, and B. J. Cantwell, 1990: A general classification of three-dimensional flow fields. *Phys. Fluids,* **2A,** 765–777.

Chumakov, S. G., 2006: Statistics of subgrid-scale stress states in homogeneous isotropic turbulence. *J. Fluid Mech.,* **562,** 405–414.

Clark, R. A., J. H. Ferziger, and W. C. Reynolds, 1979: Evaluation of subgrid models using an accurately simulated turbulent flow. *J. Fluid Mech.,* **91,** 1–16.

Deardorff, J. W., 1970: A numerical study of three-dimensional turbulent channel flow at large Reynolds numbers. *J. Fluid Mech.,* **41,** 453–480.

——, 1972: Numerical investigation of neutral and unstable planetary boundary layers. *J. Atmos. Sci.,* **29,** 91–115.

——, 1974: Three-dimensional numerical study of the height and mean structure of a heated planetary boundary layer. *Bound.-Layer Meteor.,* **29,** 91–115.

Germano, M., 1986: A proposal for a redefinition of the turbulent stresses in the filtered Navier-Stokes equations. *Phys. Fluids,* **29,** 2323–2324.

——, U. Piomelli, P. Moin, and W. H. Cabot, 1991: A dynamic subgrid-scale eddy viscosity model. *Phys. Fluids,* **3A,** 1760–1765.

Higgins, C. W., M. B. Parlange, and C. Meneveau, 2003: Alignment trends of velocity gradients and subgrid-scale fluxes in

the turbulent atmospheric boundary layer. *Bound.-Layer Meteor.,* **109,** 59–83.

Horst, T. W., J. Kleissl, D. H. Lenschow, C. Meneveau, C.-H. Moeng, M. B. Parlange, P. P. Sullivan, and J. C. Weil, 2004: HATS: Field observations to obtain spatially filtered turbulence fields from crosswind arrays of sonic anemometers in the atmospheric surface layer. *J. Atmos. Sci.,* **61,** 1566–1581.

Hunt, J., A. Wray, and P. Moin, 1988: Eddies, streams, and convergence zones in turbulent flows. *Proc. CTR Summer Program,* Stanford, CA, Center for Turbulence Research, 193–208.

Kang, H. S., and C. Meneveau, 2005: Effect of large-scale coherent structures on subgrid-scale stress and strain-rate eigenvector alignments in turbulent shear flow. *Phys. Fluids,* **17,** 055103, doi:10.1063/1.1890425.

Kleissl, J., C. Meneveau, and M. B. Parlange, 2003: On the magnitude and variability of subgrid-scale eddy-diffusion coefficients in the atmospheric surface layer. *J. Atmos. Sci.,* **60,** 2372–2388.

——, M. B. Parlange, and C. Meneveau, 2004: Field experimental study of dynamic Smagorinsky models in the atmospheric surface layer. *J. Atmos. Sci.,* **61,** 2296–2307.

——, V. Kumar, C. Meneveau, and M. B. Parlange, 2006: Numerical study of dynamic Smagorinsky models in large-eddy simulation of the atmospheric boundary layer: Validation in stable and unstable conditions. *Water Resour. Res.,* **42,** W06D10, doi:10.1029/2005WR004685.

Kobayashi, H., 2005: The subgrid-scale models based on coherent structures for rotating homogeneous turbulence and turbulent channel flow. *Phys. Fluids,* **17,** 045104, doi:10.1063/1.1874212.

Kosovic, B., 1997: Subgrid-scale modelling for the large-eddy simulation of high-Reynolds-number boundary layers. *J. Fluid Mech.,* **336,** 151–182.

Kumar, V., J. Kleissl, C. Meneveau, and M. B. Parlange, 2006: Large-eddy simulation of a diurnal cycle of the turbulent atmospheric boundary layer: Atmospheric stability and scaling issues. *Water Resour. Res.,* **42,** W06D09, doi:10.1029/2005WR004651.

Langford, J. A., and R. D. Moser, 1999: Optimal LES formulations for isotropic turbulence. *J. Fluid Mech.,* **398,** 321–346.

Leith, C. E., 1990: Stochastic backscatter in a subgrid-scale model: Plane shear mixing layer. *Phys. Fluids,* **2A,** 297–299.

Lilly, D. K., 1967: The representation of small-scale turbulence in numerical simulation experiments. *Proc. IBM Scientific Computing Symp. on Environmental Sciences,* Yorktown Heights, NY, IBM, 195–209.

Lin, C. L., 1999: Near-grid-scale energy transfer and coherent structures in the convective planetary boundary layer. *Phys. Fluids,* **11,** 3482–3494.

Lund, T. S., and E. Novikov, 1992: Parameterization of subgrid-scale stress by the velocity gradient tensor. Center for Turbulence Research Annual Research Brief, Stanford University.

——, and M. M. Rogers, 1994: An improved measure of strain state probability in turbulent flows. *Phys. Fluids,* **6,** 1838–1847.

Machiels, L., 1997: Predictability of small-scale motion in isotropic fluid turbulence. *Phys. Rev. Lett.,* **79,** 3411–3414.

Majda, A. J., and M. G. Shefter, 1998: Elementary stratified flows with instability at large Richardson number. *J. Fluid Mech.,* **376,** 319–350.

Martín, J., C. Dopazo, and L. Valiño, 1998: Dynamics of velocity gradient invariants in turbulence: Restricted Euler and linear diffusion models. *Phys. Fluids,* **10,** 2012–2025.

Mason, P. J., 1994: Large-eddy simulation: A critical review. *Quart. J. Roy. Meteor. Soc.,* **120,** 1–26.

——, and D. J. Thomson, 1992: Stochastic backscatter in large-eddy simulations of boundary layers. *J. Fluid Mech.,* **242,** 51–78.

Meneveau, C., and J. Katz, 1999: Conditional subgrid force and dissipation in locally isotropic and rapidly strained turbulence. *Phys. Fluids,* **11,** 2317–2329.

——, and ——, 2000: Scale-invariance and turbulence models for large-eddy simulation. *Annu. Rev. Fluid Mech.,* **32,** 1–32.

——, T. S. Lund, and W. H. Cabot, 1996: A Lagrangian dynamic subgrid-scale model of turbulence. *J. Fluid Mech.,* **319,** 353–385.

Moeng, C.-H., 1984: A large-eddy-simulation model for the study of planetary boundary-layer turbulence. *J. Atmos. Sci.,* **41,** 2052–2062.

Pope, S. B., 1975: A more general effective-viscosity hypothesis. *J. Fluid Mech.,* **72,** 331–340.

Porté-Agel, F., C. Meneveau, and M. B. Parlange, 2000: A scale-dependent dynamic model for large-eddy simulation: Application to a neutral atmospheric boundary layer. *J. Fluid Mech.,* **415,** 261–284.

——, M. Pahlow, C. Meneveau, and M. B. Parlange, 2001a: Atmospheric stability effect on subgrid-scale physics for large-eddy simulation. *Adv. Water Res.,* **24,** 1085–1102.

——, M. B. Parlange, C. Meneveau, and W. E. Eichinger, 2001b: A priori field study of the subgrid-scale heat fluxes and dissipation in the atmospheric surface layer. *J. Atmos. Sci.,* **58,** 2673–2698.

Schumann, U., 1975: Subgrid scale model for finite difference simulations of turbulent flows in plane channels and annuli. *J. Comput. Phys.,* **18,** 376–404.

Shtilman, L., M. Spector, and A. Tsinober, 1993: On some kinematic versus dynamic properties of homogeneous turbulence. *J. Fluid Mech.,* **247,** 65–77.

Smagorinsky, J., 1963: General circulation experiments with the primitive equations. Part I: The basic experiment. *Mon. Wea. Rev.,* **91,** 99–164.

Sullivan, P. P., J. C. McWilliams, and C. H. Moeng, 1994: A subgrid-scale model for large-eddy simulation of planetary boundary layer flows. *Bound.-Layer Meteor.,* **71,** 247–276.

——, T. W. Horst, D. H. Lenschow, C.-H. Moeng, and J. C. Weil, 2003: Structure of subfilter-scale fluxes in the atmospheric surface layer with application to large-eddy simulation modelling. *J. Fluid Mech.,* **482,** 101–139.

Tao, B., J. Katz, and C. Meneveau, 2002: Statistical geometry of subgrid-scale stresses determined from holographic particle image velocimetry measurements. *J. Fluid Mech.,* **457,** 35–78.

Tong, C., J. C. Wyngaard, and J. G. Brasseur, 1999: Experimental study of the subgrid-scale stresses in the atmospheric surface layer. *J. Atmos. Sci.,* **56,** 2277–2292.